







Direct evidence of magnetization rotation at the ferromagnetic morphotropic phase boundary in $\text{Tb}_{1-x}\text{Dy}_x\text{Fe}_2$ system

Xiaoqin Ke ¹, Chao Zhou ¹, Ben Tian,¹ Yoshitaka Matsushita ², Xiaobing Ren ³, Sen Yang ^{1,*} and Yunzhi Wang ⁴

¹*School of Physics, MOE Key Laboratory for Nonequilibrium Synthesis and Modulation of Condensed Matter, State Key Laboratory for Mechanical Behavior of Materials, Xi'an Jiaotong University, Xi'an 710049, China*

²*National Institute for Materials Science, Beamline BL15XU, Spring-8, 1-1-1 Kohto, Sayo-cho, Hyogo 679-5148, Japan*

³*Ferroic Physics Group, National Institute for Materials Science, Tsukuba 305-0047, Ibaraki, Japan*

⁴*Department of Materials Science and Engineering, The Ohio State University, Columbus, Ohio 43210, USA*



(Received 20 June 2023; accepted 27 November 2023; published 13 December 2023)

The large magnetostriction at the ferromagnetic morphotropic phase boundary (MPB) relies on easy magnetization switching under external magnetic fields. It has been proposed that both domain wall motion and magnetization rotation occur under external magnetic fields at the ferromagnetic MPB. However, direct experimental evidence of the latter is still lacking. Here we report direct evidence of both magnetization rotation and domain wall motion under an external magnetic field at the MPB of the $\text{Tb}_{1-x}\text{Dy}_x\text{Fe}_2$ system through *in situ* synchrotron x-ray diffraction experiments, which are further confirmed by phase field simulations. This work unravels the origin of the large magnetostriction at the ferromagnetic MPB and could shed light on the design of magnetostrictive materials.

DOI: [10.1103/PhysRevB.108.224419](https://doi.org/10.1103/PhysRevB.108.224419)

I. INTRODUCTION

The ferromagnetic morphotropic phase boundary (MPB), which was initially called the “spin reorientation boundary” [1], refers to the phase boundary separating a tetragonal structure with [001] easy magnetization direction, and a rhombohedral structure with [111] easy magnetization direction in the phase diagram of ferromagnetic systems [2,3]. Such a ferromagnetic MPB has been found in a number of binary ferromagnetic systems, such as $\text{Tb}_{1-x}\text{Dy}_x\text{Fe}_2$, $\text{Tb}_{1-x}\text{Dy}_x\text{Co}_2$, and $\text{Tb}_{1-x}\text{Gd}_x\text{Fe}_2$ [2–5]. Similar to the giant piezoelectricity at the ferroelectric MPB [6,7], giant magnetostriction has been reported at the ferromagnetic MPB [2,3], which could find application in a wide range of devices such as sensors, actuators, transducers, and sonar, and thus has attracted much attention in recent years.

The magnetostriction of ferromagnetic materials is underpinned by magnetic domain switching under an external magnetic field. Therefore, to understand the giant magnetostriction at the ferromagnetic MPB, it is essential to know how domain switching occurs under external magnetic fields at the MPB. Similar to physically parallel ferroelectric MPB systems, where two possible domain-switching models exist, i.e., polarization domain wall motion [8] and polarization rotation [9], there are also two existing domain-switching models at ferromagnetic MPBs, i.e., magnetic domain wall motion and magnetization rotation [1,3–5,10–17]. While the magnetic domain wall motion mechanism has been theoretically predicted and experimentally confirmed [10–13], there has been no direct experimental evidence to support the magnetization rotation mechanism, although it was proposed

theoretically over 50 years ago [1,17]. This may greatly hinder the understanding of the origin of the large magnetostriction at ferromagnetic MPBs.

One possible way to detect the magnetization rotation experimentally under external magnetic fields is to measure the lattice parameter change under external fields, as the crystal lattice structure is directly coupled to the magnetization direction [18]. However, unlike the strong polarization-lattice coupling in ferroelectric systems and thus large lattice distortion at ferroelectric phase transitions [19], ferromagnetic materials generally show very small lattice distortion at ferromagnetic phase transitions due to the weak spin-lattice coupling in ferromagnetic systems [18]. Thus, it has remained a big challenge to detect magnetization rotation experimentally.

In this work, we consider the well-known ferromagnetic MPB system $\text{Tb}_{1-x}\text{Dy}_x\text{Fe}_2$ [3,16,17,20] and carry out *in situ* high-resolution synchrotron x-ray diffraction (XRD) measurements on the ferromagnetic MPB composition at different temperatures with 0 and 4 kOe external magnetic fields. We found that under the external magnetic field, only domain wall motion occurs at temperatures far away from the MPB, as evidenced by the intensity change of characteristic XRD peaks without any shift of peak positions. However, at temperatures near the MPB, in addition to domain wall motion, magnetization rotation also occurs, which is supported by the position shift of characteristic XRD peaks. Further phase field simulations have confirmed that both domain wall motion and magnetization rotation occur at the ferromagnetic MPB due to the small magnetization anisotropy. This work unravels the mechanism of domain switching at ferromagnetic MPBs and could shed light on the design of new magnetostrictive materials.

*Corresponding author: yang.sen@mail.xjtu.edu.cn

II. METHODS

A. Experimental methods

$\text{Tb}_{1-x}\text{Dy}_x\text{Fe}_2$ alloys ($x = 0.0$ to 1.0) were prepared by arc melting from high-purity (99.9%) terbium, dysprosium, and iron in an argon atmosphere. The crystal structure was observed by high-resolution synchrotron XRD at the BL15XU NIMS beamline in Spring-8. The samples for XRD measurement were first ground into powder and then sealed into quartz capillaries with a diameter of 1 mm. During the XRD measurements, the capillaries were rotated so that the effect of possible preferred orientation could be reduced and the diffraction density could be averaged. During XRD measurements, the temperatures of the samples were controlled to vary between 40 and 400 K by a blow-type cryocooler, and the external magnetic fields were applied through a NdFeB permanent magnet placed under the rotating sample [18]. The magnetic properties of the samples were tested by a superconducting quantum interference device, and the magnetostriction of them was measured utilizing strain gauges. The storage modulus of the samples was measured by the dynamic mechanical analysis (DMA) equipment at a frequency of 1 Hz.

B. Phase field simulation methods

Phase field simulations of a $\text{Tb}_{0.3}\text{Dy}_{0.7}\text{Fe}_2$ single-crystalline sample were performed. The magnetization vector of each domain in the system is represented by \mathbf{M} ($\mathbf{M} = M_S \mathbf{m}$), in which M_S is the saturation magnetization and \mathbf{m} (m_1, m_2, m_3) is the unit vector describing the magnetization direction. The total free energy of the system F_{total} is written as the sum of the magnetocrystalline anisotropy energy F_{ani} , the exchange energy F_{exch} , the magnetostatic energy F_{mag} , the external magnetic energy F_{ex} , and the elastic energy F_{el} , i.e., $F_{\text{total}} = F_{\text{ani}} + F_{\text{exch}} + F_{\text{mag}} + F_{\text{ex}} + F_{\text{el}}$. The magnetocrystalline anisotropy energy density f_{ani} is written as a function of (m_1, m_2, m_3) ,

$$f_{\text{ani}} = K_1(m_1^2 m_2^2 + m_1^2 m_3^2 + m_2^2 m_3^2) + K_2 m_1^2 m_2^2 m_3^2, \quad (1)$$

where K_1 and K_2 are the magnetocrystalline anisotropy coefficients. The exchange energy density f_{exch} is written in terms of \mathbf{m} as follows: $f_{\text{exch}} = A \sum_{i,j=1,2,3} (m_{i,j})^2$. The magnetostatic energy density f_{mag} is calculated by $f_{\text{mag}} = -\frac{1}{2} \mu_0 M_S (\mathbf{H}_{\text{d}}^{\text{tot}} \cdot \mathbf{m})$, in which the total stray field $\mathbf{H}_{\text{d}}^{\text{tot}}$ is the sum of the long-range spin-spin interaction field $\mathbf{H}_{\text{d}}^{\text{hetero}}$ and the demagnetization field $\mathbf{H}_{\text{d}}^{\text{shape}}$. $\mathbf{H}_{\text{d}}^{\text{hetero}}$ is solved by the magnetostatic equilibrium equation $\nabla \cdot (\mu_0 \mathbf{H}_{\text{d}}^{\text{hetero}} + \mu_0 M_S \mathbf{m}) = 0$. The external magnetic energy density f_{ex} is written as $f_{\text{ex}} = -\mu_0 M_S \mathbf{H}_{\text{ex}} \cdot \mathbf{m}$, where \mathbf{H}_{ex} is the external magnetic field. The elastic energy density f_{el} is calculated by $f_{\text{el}} = \frac{1}{2} c_{ijkl} e_{ij} e_{kl} = \frac{1}{2} c_{ijkl} (\varepsilon_{ij} - \varepsilon_{ij}^0) (\varepsilon_{kl} - \varepsilon_{kl}^0)$, where c_{ijkl} is the elastic stiffness tensor, e_{ij} is the elastic strain, ε_{ij} is the total strain, and ε_{ij}^0 is the spontaneous strain or stress-free strain. The stress-free strain can be calculated as

$$\begin{aligned} \varepsilon_{11}^0 &= \frac{3}{2} \lambda_{100} (m_1^2 - \frac{1}{3}), & \varepsilon_{12}^0 &= \frac{3}{2} \lambda_{111} m_1 m_2 \\ \varepsilon_{22}^0 &= \frac{3}{2} \lambda_{100} (m_2^2 - \frac{1}{3}), & \varepsilon_{13}^0 &= \frac{3}{2} \lambda_{111} m_1 m_3 \\ \varepsilon_{33}^0 &= \frac{3}{2} \lambda_{100} (m_3^2 - \frac{1}{3}), & \varepsilon_{23}^0 &= \frac{3}{2} \lambda_{111} m_2 m_3, \end{aligned} \quad (2)$$

where λ_{100} and λ_{111} are the magnetostrictive coefficients of a cubic crystal.

The magnetization evolution is then obtained by solving the time-dependent Ginzburg-Landau equation $\frac{\partial \mathbf{m}}{\partial t} = -L \frac{\delta F_{\text{total}}}{\delta \mathbf{m}}$ [21], where L is the kinetic coefficient. The parameters used in our simulations are $M_S = 8.0 \times 10^5$ A/m, $K_1 = -1.2 \times 10^4$ (T/K-250) J/m³ (in which T is the temperature), $K_2 = 0$, $\lambda_{100} = 100$ ppm, $\lambda_{111} = 1600$ ppm, $c_{11} = 1.41 \times 10^{11}$ N/m², $c_{12} = 6.48 \times 10^{10}$ N/m², and $c_{44} = 4.87 \times 10^{10}$ N/m² [22]. The simulations were carried out in two dimensions with cell sizes of 512×512 grids. Periodic boundary conditions were applied in both dimensions. The time-dependent Ginzburg-Landau equation was solved by the semi-implicit Fourier spectral method.

III. RESULTS AND DISCUSSION

A. Full phase diagram of the $\text{Tb}_{1-x}\text{Dy}_x\text{Fe}_2$ system and the magnetostrictive properties at the MPB

Figure 1(a) shows the temperature-composition phase diagram of the $\text{Tb}_{1-x}\text{Dy}_x\text{Fe}_2$ system, which was constructed using magnetization-temperature curves of all compositions combined with the ac susceptibility (χ')-temperature curves and synchrotron XRD profiles of MPB compositions. Note that although extensive work has been done on this ferromagnetic MPB system [3,16,17,20], this is the first time that a complete phase diagram has been constructed. The phase diagram consists of four regions: a high-temperature cubic-phase (C, paramagnetic) region, a low-temperature rhombohedral-phase (R, easy magnetization direction $\langle 111 \rangle$) region, a low-temperature tetragonal-phase (T, easy magnetization direction $\langle 100 \rangle$) region, and an intermediate state (IS) region in between the R- and T-phase regions. The Curie temperatures (T_C) of all compositions in the phase diagram are determined from the magnetization-temperature curves of different compositions, as exemplified by that of $\text{Tb}_{0.3}\text{Dy}_{0.7}\text{Fe}_2$ given in Fig. 1(b). The R-to-T phase transition temperatures of MPB compositions (T_{MPB}) are obtained from the ac susceptibility (χ') versus temperature relations as exemplified by that of $\text{Tb}_{0.3}\text{Dy}_{0.7}\text{Fe}_2$ given in Fig. 1(c). The inset in Fig. 1(c) also shows the storage modulus-versus-temperature curve of $\text{Tb}_{0.3}\text{Dy}_{0.7}\text{Fe}_2$, where the storage modulus exhibits a dip at T_{MPB} , indicating elastic softening at the MPB, and is similar to the elastic softening found at ferroelectric MPBs [23]. The red shaded area at the MPB line corresponds to an IS between the R- and T-phase regions detected by the synchrotron XRD results given in Fig. 1(d), which shows that, with temperature decreasing, the {440} diffraction pattern evolves from that of R (two {440} peaks) at 300 K to that of T (one {440} peak only due to the too small tetragonal distortion here) at 160 K through that of an intermediate state (three {440} peaks) near T_{MPB} (between 250 K and 220 K).

The three {440} peaks appearing in the IS region of the phase diagram could arise from the presence of either a mixture of R and T phases [3] or a mixture of R (or T) and monoclinic (M) phases. Figure 2 shows the comparison of the XRD Rietveld refinement results by the model of T + R mixture and the model of R + M mixture for {440} peaks at 250 K, which illustrates that the values of goodness-of-fit

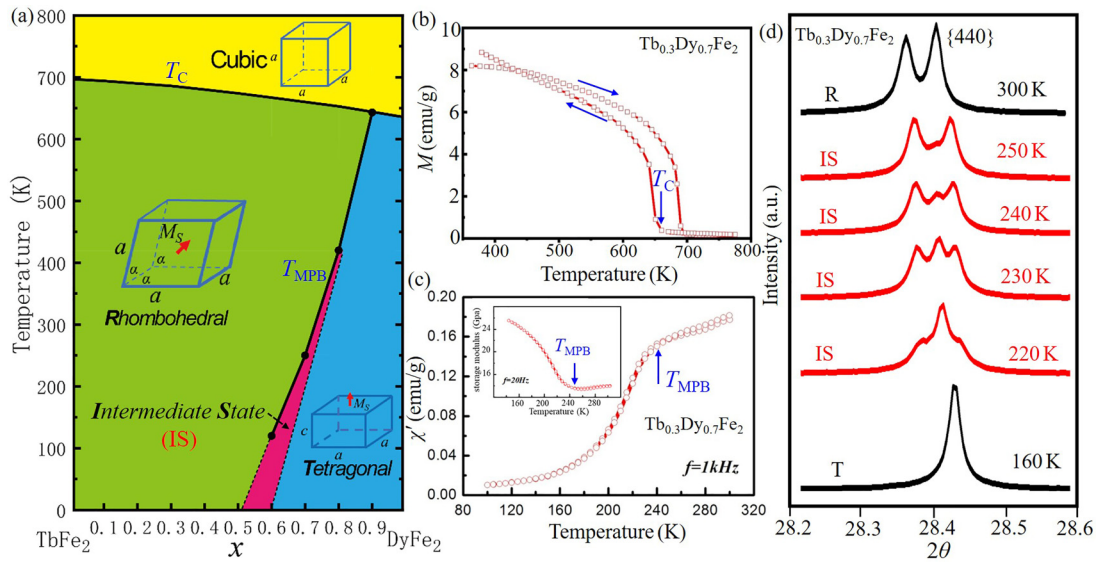


FIG. 1. (a) Full phase diagram of $Tb_xDy_{1-x}Fe_2$ system. (b) M - T curves of one representative MPB composition: $Tb_{0.3}Dy_{0.7}Fe_2$. (c) ac Susceptibility (χ') versus T curve of $Tb_{0.3}Dy_{0.7}Fe_2$. Inset: Storage modulus versus T curve of $Tb_{0.3}Dy_{0.7}Fe_2$. (d) The synchrotron XRD results at the $\{440\}$ peaks at different temperatures for $Tb_{0.3}Dy_{0.7}Fe_2$.

(χ^2) and Rietveld indices (Rwp) are small for both models. Thus, it is difficult to distinguish whether the new M phase

exists at the MPB through the synchrotron XRD results at zero-field only. However, both the phase field simulation results and the synchrotron XRD data under external magnetic fields given later suggest the presence of the new M phase. Also note that for typical ferroelectric MPB systems, such as $PbMg_{1/3}Nb_{2/3}O_3-xPbTiO_3$ and $PbZrO_3-xPbTiO_3$, both experiments and theoretical models have indicated the presence of the M phase at the MPBs [9,24].

Figure 3(a1) and 3(b1) shows the measured strain-magnetic field loops at different temperatures and the strain-temperature curves for $Tb_{0.3}Dy_{0.7}Fe_2$ under an external magnetic field of 10 kOe and 50 kOe, respectively. Figure 3(a2) and 3(b2) summarizes the variation of its magnetostriction at these two fields with temperature. It indicates that under an external magnetic field of 10 kOe, the largest magnetostriction occurs at ~ 220 K and reaches a value over

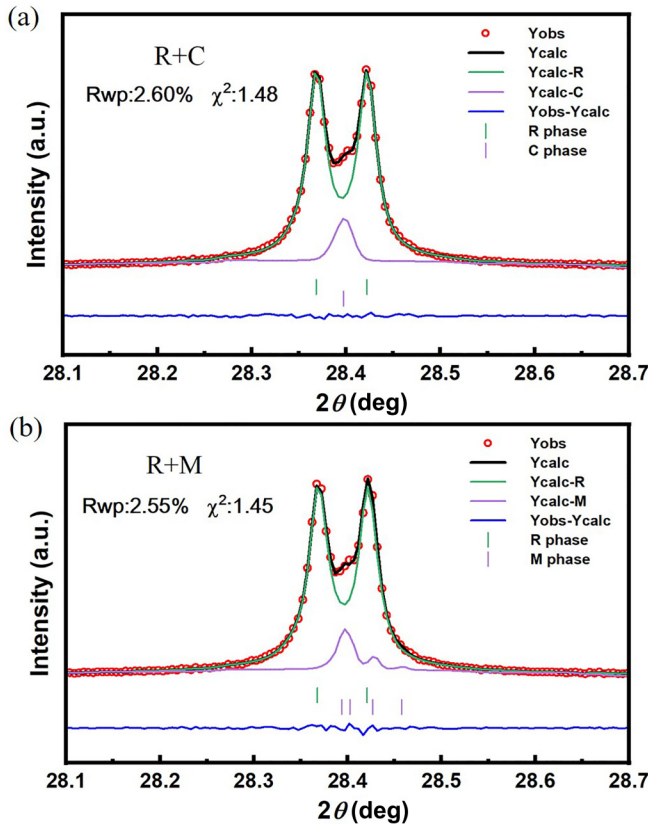


FIG. 2. Comparison of results of the XRD Rietveld refinement by the model of the R + T mixture (a) and the model of the R + M mixture (b). Note that, here, the C phase instead of the T phase is used for fitting because the tetragonal distortion in the $Tb_{1-x}Dy_xFe_2$ system is too small to be resolved by synchrotron XRD.

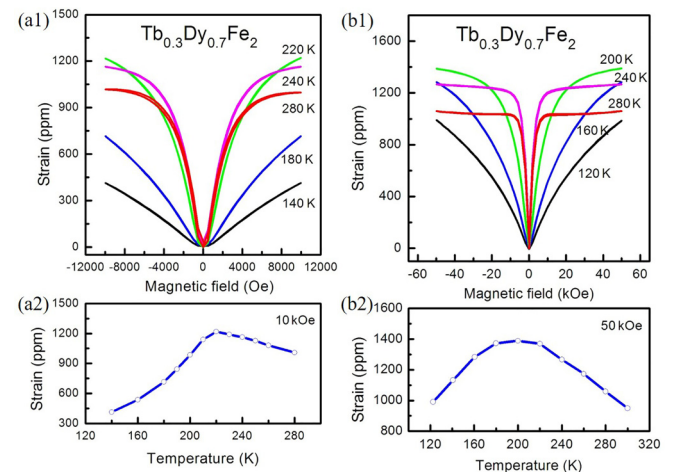


FIG. 3. The magnetostriction of $Tb_{0.3}Dy_{0.7}Fe_2$ at different temperatures under an external field of 10 kOe [(a1) and (a2)] and 50 kOe [(b1) and (b2)].

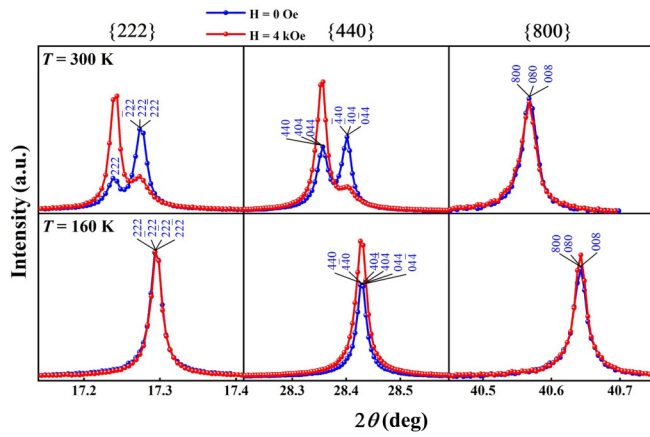


FIG. 4. The {222}, {440}, and {800} peak profiles of $\text{Tb}_{0.3}\text{Dy}_{0.7}\text{Fe}_2$ at 0 Oe and 4 kOe external magnetic fields at temperatures in the R-phase region ($T = 300$ K) and T-phase region ($T = 160$ K). In the T-phase region ($T = 160$ K), theoretically both the {440} and {800} peaks were supposed to split into two peaks with an intensity ratio of 1:2 and 2:1, respectively. But here, the peak splitting does not occur because the tetragonal distortion in the system is too small to be detected.

1200 ppm. Under a larger external magnetic field of 50 kOe, the largest magnetostriction occurs at a lower temperature of ~ 200 K and reaches a value of ~ 1400 ppm. Therefore, it is clear that the largest magnetostriction appears near the MPB (at the IS region) of the $\text{Tb}_{1-x}\text{Dy}_x\text{Fe}_2$ phase diagram.

B. Direct evidence of magnetization rotation at the MPB composition ($\text{Tb}_{0.3}\text{Dy}_{0.7}\text{Fe}_2$) detected by synchrotron XRD experiments

If magnetization rotation occurs under an external magnetic field, lattice distortion would be induced due to the magnetoelastic coupling effect, as shown by Eq. (2). It can be deduced from Eq. (2) that, if the magnetization direction is along the [001] direction, $\varepsilon_{11}^0 = \varepsilon_{22}^0 \neq \varepsilon_{33}^0$ and $\varepsilon_{12}^0 = \varepsilon_{13}^0 = \varepsilon_{23}^0$. Such a lattice distortion produces a tetragonal symmetry. When the magnetization direction is along the [111] direction, $\varepsilon_{11}^0 = \varepsilon_{22}^0 = \varepsilon_{33}^0 = 0$ and $\varepsilon_{12}^0 = \varepsilon_{13}^0 = \varepsilon_{23}^0 \neq 0$, which corresponds to a rhombohedral symmetry. When the magnetization direction is along the [110] direction, $\varepsilon_{11}^0 = \varepsilon_{22}^0 \neq \varepsilon_{33}^0$, $\varepsilon_{12}^0 \neq 0$, and $\varepsilon_{13}^0 = \varepsilon_{23}^0 = 0$, which corresponds to an orthorhombic symmetry. Finally, when the magnetization direction is along the [uuv] or [0uv] direction, $\varepsilon_{11}^0 = \varepsilon_{22}^0 \neq \varepsilon_{33}^0$ and $\varepsilon_{12}^0 \neq \varepsilon_{13}^0 \neq \varepsilon_{23}^0$, which corresponds to a monoclinic symmetry. Therefore, in order to find direct evidence of magnetization rotation, we then investigate the domain-switching mechanism of the $\text{Tb}_{0.3}\text{Dy}_{0.7}\text{Fe}_2$ MPB composition through comparison of synchrotron XRD peaks under a zero and finite magnetic field.

Figure 4 shows the selected regions of *in situ* synchrotron XRD patterns obtained both under a zero field and under a 4-kOe field at 300 K (in the R-phase region) and 160 K (in the T-phase region), which demonstrate that at 300 K, the intensity ratio for the (222)/(222̄) peaks shows a large increase after the external magnetic field is applied. This intensity change is due to the domain reorientation through domain wall motion, which is also reflected in the increased (440)/(440̄)

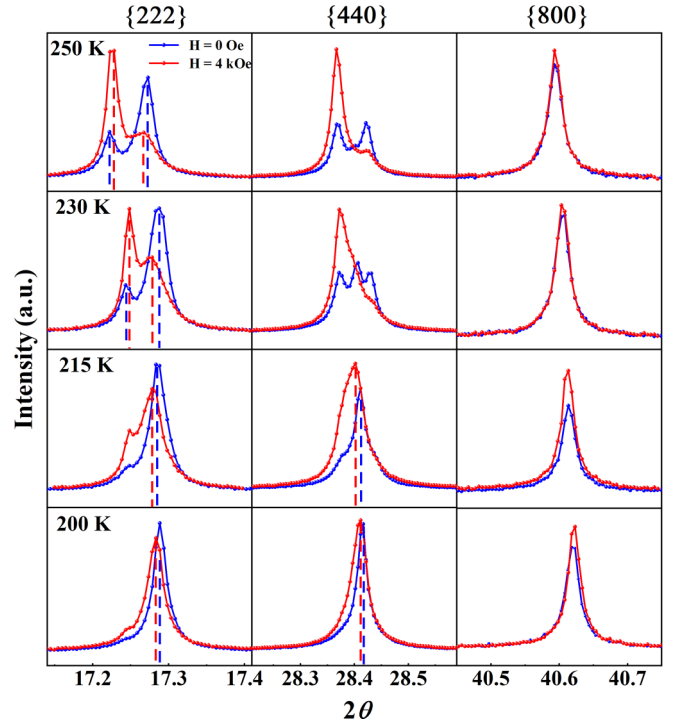


FIG. 5. The {222}, {440}, and {800} reflections for the $\text{Tb}_{0.3}\text{Dy}_{0.7}\text{Fe}_2$ alloy at zero external field and under a field of 4 kOe at temperatures in the intermediate state region (at 250 K, 230 K, 215 K, and 200 K).

peak intensity ratio [18]. On the other hand, these XRD patterns also show that the positions of all three characteristic peaks do not shift, which suggests that the lattice parameter of the crystal lattice does not change. Similarly, at 160 K, no peak shift occurs before and after the external magnetic field is applied, thus also suggesting no lattice parameter change. Therefore, at temperatures far away from the MPB, both in the R- and T-phase regions, the external magnetic field reorients the domains through domain wall motion but does not change the lattice parameter.

However, at temperatures close to the MPB, the situation is different. Figure 5 illustrates the selected regions of the XRD patterns of $\text{Tb}_{0.3}\text{Dy}_{0.7}\text{Fe}_2$ both under zero magnetic field and under a magnetic field of 4 kOe at 250 K, 230 K, 215 K, and 200 K, respectively. As illustrated in Figure 1, at these temperatures the structure of the sample at zero external magnetic field is in the IS region. Under the external magnetic field of 4 kOe, it is demonstrated that at all four temperatures, the intensity ratio of the {222} and {440} peaks changes significantly, which thus indicates that domain wall motion occurs at all four temperatures. Furthermore, shifts of peak positions have also been detected, which indicates that lattice distortion and thus magnetization rotation through the M phase occur at all four temperatures. Note that at 250 K and 230 K, only the positions of the {222} peaks shift for an appreciable amount while at 215 K and 200 K, both the {222} peak and the {440} peak shift. Such a difference could be due to the fact that at higher temperatures (250 K and 230 K) that are closer to the R-phase region, the magnetization vector rotates through the M_B phase with a [vu] ($v < u$) easy

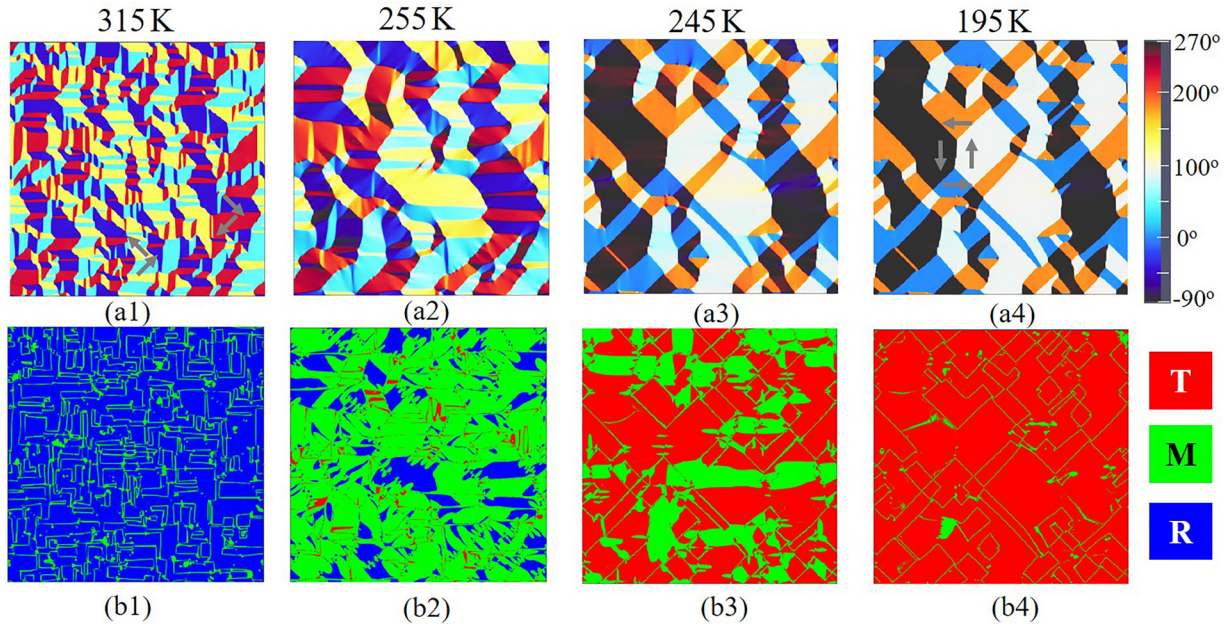


FIG. 6. Evolution of domain structure and phases with temperature decreasing for the $\text{Tb}_{0.3}\text{Dy}_{0.7}\text{Fe}_2$ alloy obtained by phase field simulations. (a1)–(a4) Domain structure. Different colors represent the angle between the magnetization vector and the horizontal axis (θ), as indicated by the color bar. (b1)–(b4) The distribution of the T, M, and R phases in the sample.

magnetization direction within the (011) plane, while at lower temperatures (215 K and 200 K) that are closer to the T-phase region, the magnetization vector rotates through M_C phase with the [0uv] easy direction within the (001) plane [25,26]. Also note that no peak shifts are detected for the {800} peaks at all four temperatures because λ_{100} is extremely small in this system [3]. Therefore, the synchrotron XRD results given in Fig. 5 demonstrate that near the T_{MPB} of the $\text{Tb}_{0.3}\text{Dy}_{0.7}\text{Fe}_2$ alloy, both magnetization rotation and domain wall motion occur under external magnetic fields.

C. Confirmation of magnetization rotation mechanism at the ferromagnetic MPB by phase field simulations

In order to illustrate the details of the previous two magnetization switching processes, two-dimensional (2D) phase field simulations are performed. Figure 6(a1)–6(a4) shows the simulated domain structures in $\text{Tb}_{0.3}\text{Dy}_{0.7}\text{Fe}_2$ at different temperatures, represented by the magnetization direction θ of each domain at each grid point, where θ is defined as the angle between the magnetization vector \mathbf{m} and the horizontal direction. Figure 6(b1)–6(b4) illustrates the distribution of the T, R, and M phases within the whole sample at different temperatures. These simulation results clearly illustrate that, upon cooling, the domain structure of the sample changes from one with R domains [Fig 6(a1) and 6(b1)] to a mixture of M + R domains [Fig 6(a2) and 6(b2)], and then to a mixture of M + T domains [Fig 6(a3) and 6(b3)], and finally to one with T domains [Fig 6(a4) and 6(b4)], which suggests that the IS region detected by synchrotron XRD patterns should include the new M phase. Note that the M phase is not expected according to the magnetocrystalline anisotropy energy because the magnetocrystalline energy used in the simulations takes the form of a sixth-order polynomial with K_1 and

K_2 only [see Eq. (1)] [25–27]. However, the M phase still appears because it is stabilized by the long-range elastic energy and magnetostatic energy considered in the simulations under small magnetocrystalline anisotropy, which is similar to our previous finding that the M phase, although not stabilized by the sixth-order Landau free energy, could be stabilized by the long-range electrostatic and elastic energy under small polarization anisotropy at the ferroelectric MPB [28,29].

Figure 7(a1)–7(c2) then gives the domain structure evolution upon the application of an external magnetic field of ~ 4 kOe along vertical direction at three different temperatures (315 K, 255 K, and 195 K) and Fig. 7(a3)–7(c3) plots variations of the magnetization direction (θ) with positions along the yellow dashed lines in Fig. 7(a1)–7(c2). It is readily seen that with the application of the external magnetic field, only domain wall motion occurs at $T = 315$ K and 195 K (which are away from MPB), while both domain wall motion and magnetization rotation occur at $T = 255$ K (which is near MPB). Such phase field simulation results are qualitatively consistent with the synchrotron XRD results shown in Figs. 4 and 5.

D. Origin of magnetization rotation mechanism and its implications

To understand further why continuous magnetization rotation could occur at a ferromagnetic MPB, a simple analysis is given next. Under an external magnetic field along the x_1 direction, the total free energy density of the system (f_{total}) can be approximated as the sum of magnetocrystalline anisotropy energy and the Zeeman energy, i.e., $f_{\text{total}} = K_1 m_1^2 m_2^2 - \mu_0 M_s H_1 m_1 = K_1 \cos^2 \theta \sin^2 \theta - h_1 \cos \theta$, where $h_1 = \mu_0 M_s H_1$ (2D case), and it can be shown that when K_1 is large ($K_1 = K_0 > 0$), the stable phase is always the T phase ($\theta = 0^\circ$) both

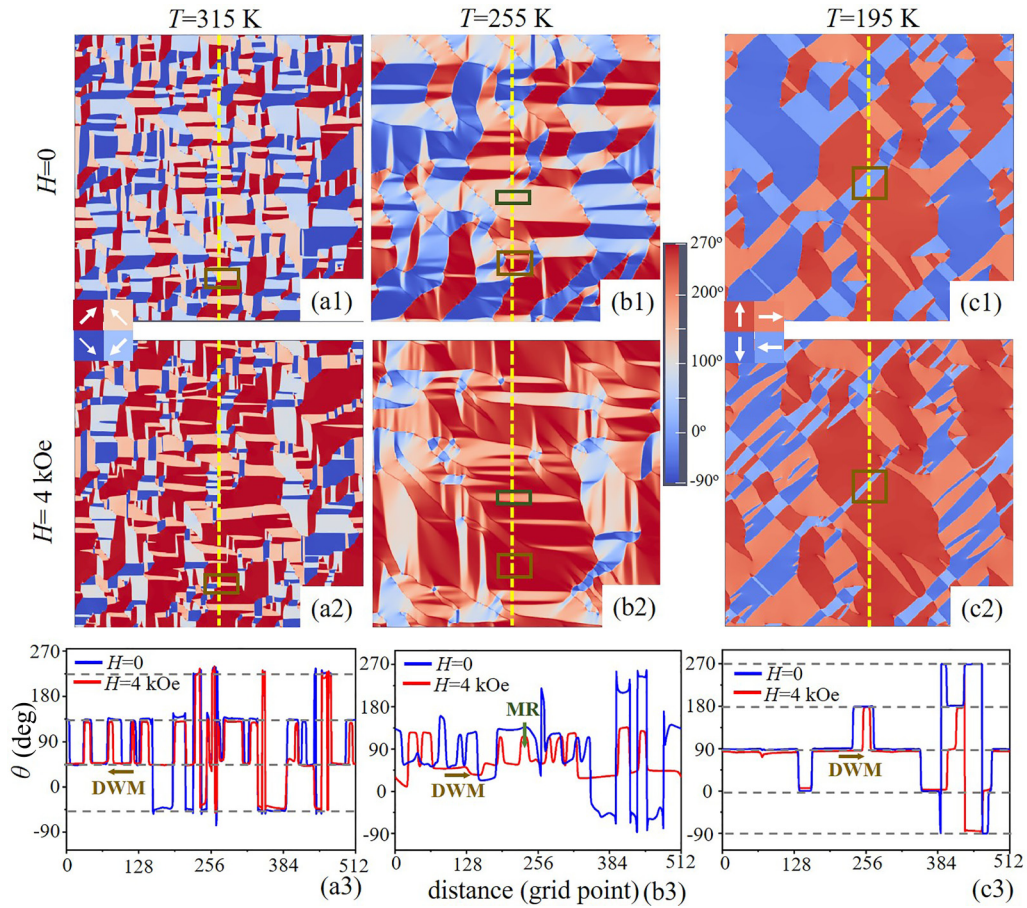


FIG. 7. (a1)–(c1) The domain structure at $H = 0$ kOe. (a2)–(c2) The domain structure at $H = 4$ kOe. (a3)–(c3) Variation of θ with distance along the yellow dashed line in (a1)–(c1) and (a2)–(c2). MR and DWM are the abbreviation of magnetization rotation and domain wall motion, respectively. The dark-gold and dark-green solid rectangles in (a1)–(c1) and (a2)–(c2) give the positions where DMW and MR, represented by the arrows in (a3)–(c3) occur, respectively.

without and with an external magnetic field H_1 , as shown in Fig. 8(a); but when K_1 is small ($K_1 = 0.1K_0$), the external magnetic field of H_1 would rotate the magnetization from the easy [01] direction ($\theta = 90^\circ$, T phase) to the [uv] direction ($45^\circ < \theta < 90^\circ$, M phase), as shown in Fig. 8(b). Therefore, at the ferromagnetic MPB where the magnetocrystalline anisotropic energy coefficient is small, magnetization rotation under external magnetic fields could occur.

Note that at a ferroelectric MPB, continuous polarization rotation also occurs due to the small polarization anisotropy [9,29]. It thus can be concluded that continuous rotation of the order parameter vector could be a general domain-switching mechanism in ferroic materials with small anisotropy. The conventional domain-switching mechanism, i.e., domain wall motion, occurs in ferroic materials with relatively large anisotropy. At small anisotropy, both domain wall motion and

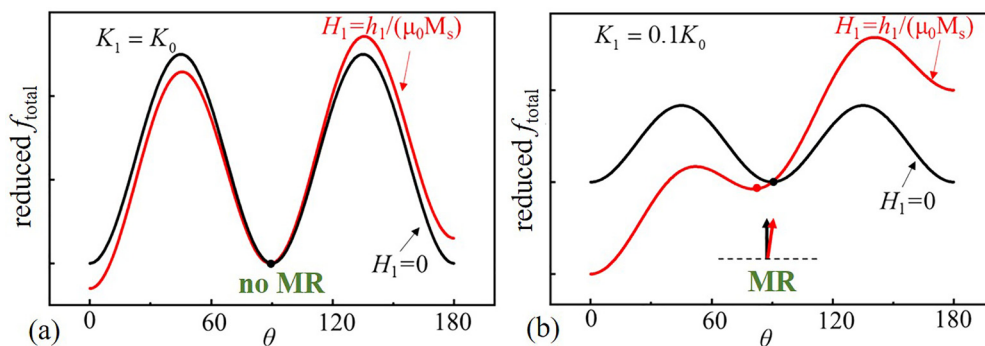


FIG. 8. Variation of magnetization direction (θ) under the same external magnetic field at large anisotropy ($K_1 = K_0$) (a) and small anisotropy ($K_1 = 0.1K_0$) (b), respectively.

continuous rotation of order parameters could be the possible domain-switching mechanisms under external fields.

IV. CONCLUSION

In summary, we have constructed a complete phase diagram of the $Tb_xDy_{1-x}Fe_2$ system. At the MPB in between the high-temperature rhombohedral-phase region and the low-temperature tetragonal-phase region, a distinct structure and superior magnetostrictive properties are observed. Through synchrotron XRD measurements under both zero and finite magnetic fields, we find that near the MPB, both domain wall motion and magnetization rotation occur under an external magnetic field, contributing to the large magnetostriction. Further phase field simulations confirm that a monoclinic phase appears at the MPB region, and magnetization rotation could occur at the MPB due to the small magnetization anisotropy. This work suggests that rotation of the vectorial or tensorial order parameters (polarization, magnetization, and strain) could be a universal phenomenon for ferroic materials with small crystalline anisotropy that is responsible for the

appearance of a giant response at MPBs. It could shed light on the future design of high-performance ferroic materials.

ACKNOWLEDGMENTS

X.K. and S.Y. acknowledge support from the National Key Research and Development Program of China (Grants No. 2021YFB3501401 and No. 2022YFE0109500), the National Natural Science Foundation of China (Grants No. 52171189 and No. 12374120), the Key Scientific and Technological Innovation Team of Shaanxi Province (Grant No. 2020TD-001), the Innovation Capability Support Program of Shaanxi (Grants No. 2018PT-28 and No. 2017KTPT-04), the Shanghai Aerospace Science and Technology Innovation Fund (Grant No. SAST2018-117), the Fundamental Research Funds for the Central Universities (China), the World-Class Universities (Disciplines), and the Characteristic Development Guidance Funds for the Central Universities. Y.W. acknowledges support from the U.S. Natural Science Foundation (Grant No. DMR-1923929), which has facilitated this international collaboration.

-
- [1] H. Horner and C. M. Varma, Nature of spin-reorientation transitions, *Phys. Rev. Lett.* **20**, 845 (1968).
- [2] S. Yang, H. Bao, C. Zhou, Y. Wang, X. Ren, Y. Matsushita, Y. Katsuya, M. Tanaka, K. Kobayashi, X. Song, and J. Gao, Large magnetostriction from morphotropic phase boundary in ferromagnets, *Phys. Rev. Lett.* **104**, 197201 (2010).
- [3] R. Bergstrom Jr., M. Wuttig, J. Cullen, P. Zavalij, R. Briber, C. Dennis, V. O. Garlea, and M. Laver, Morphotropic phase boundaries in ferromagnets: $Tb_{1-x}Dy_xFe_2$ alloys, *Phys. Rev. Lett.* **111**, 017203 (2013).
- [4] A. Murtaza, S. Yang, M. Mi, C. Zhou, J. Wang, R. Zhang, X. Liao, Y. Wang, X. Ren, X. Song, and Y. Ren, Morphotropic phase boundary and magnetoelastic behavior in ferromagnetic $Tb_{1-x}Gd_xFe_2$ system, *Appl. Phys. Lett.* **106**, 132403 (2015).
- [5] A. Murtaza, S. Yang, T. Chang, A. Ghani, M. T. Khan, R. Zhang, C. Zhou, X. Song, M. Suchomel, and Y. Ren, Spin reorientation and magnetoelastic properties of ferromagnetic $Tb_{1-x}Nd_xCo_2$ systems with a morphotropic phase boundary, *Phys. Rev. B* **97**, 104410 (2018).
- [6] W. Liu and X. Ren, Large piezoelectric effect in Pb-free ceramics, *Phys. Rev. Lett.* **103**, 257602 (2009).
- [7] F. Li, D. Lin, Z. Chen, Z. Cheng, J. Wang, C. Li, Z. Xu, Q. Huang, X. Liao, L.-Q. Chen, T. R. Shroud, and S. Zhang, Ultrahigh piezoelectricity in ferroelectric ceramics by design, *Nat. Mater.* **17**, 349 (2019).
- [8] Y. M. Jin, Y. U. Wang, A. G. Khachatryan, J. F. Li, and D. Viehland, Conformal miniaturization of domains with low domain-wall energy: Monoclinic ferroelectric states near the morphotropic phase boundaries, *Phys. Rev. Lett.* **91**, 197601 (2003).
- [9] H. Fu and R. E. Cohen, Polarization rotation mechanism for ultrahigh electromechanical response in single-crystal piezoelectrics, *Nature (London)* **403**, 281 (2000).
- [10] A. R. Piercy, S. C. Busbridge, and D. Kendall, Application of the ratio d/χ to the investigation of magnetization processes in giant-magnetostrictive materials, *J. Appl. Phys.* **76**, 7006 (1994).
- [11] W. D. Armstrong, An incremental theory of magnetoelastic hysteresis in pseudo-cubic ferro-magnetostrictive alloys, *J. Magn. Magn. Mater.* **263**, 208 (2003).
- [12] Z. Wang, J. Liu, C. Jiang, and H. Xu, The stress-induced anisotropy in the (110) plane of the magnetostrictive $TbDyFe$ [110] oriented crystal, *J. Appl. Phys.* **108**, 063908 (2010).
- [13] B. L. Wang and Y. M. Jin, Magnetization and magnetostriction of Terfenol-D near spin reorientation boundary, *J. Appl. Phys.* **111**, 103908 (2012).
- [14] Y. Y. Huang and Y. M. Jin, Phase field modeling of magnetization processes in growth twinned Terfenol-D crystals, *Appl. Phys. Lett.* **93**, 142504 (2008).
- [15] C.-C. Hu, T.-N. Yang, H.-B. Huang, J.-M. Hu, J.-J. Wang, Y.-G. Shi, D.-N. Shi, and L.-Q. Chen, Phase-field simulation of domain structures and magnetostrictive response in $Tb_{1-x}Dy_xFe_2$ alloys near morphotropic phase boundary, *Appl. Phys. Lett.* **108**, 141908 (2016).
- [16] U. Atzmony, M. P. Dariel, and G. Dublon, Spin-orientation diagram of the pseudobinary $Tb_{1-x}Dy_xFe_2$ Laves compound, *Phys. Rev. B* **15**, 3565 (1977).
- [17] U. Atzmony, M. P. Dariel, E. R. Bauminger, D. Lebenbaum, I. Nowik, and S. Ofer, Spin-orientation diagrams and magnetic anisotropy of rare-earth-iron ternary cubic Laves compounds, *Phys. Rev. B* **7**, 4220 (1973).
- [18] S. Yang and X. Ren, Noncubic crystallographic symmetry of a cubic ferromagnet: Simultaneous structural change at the ferromagnetic transition, *Phys. Rev. B* **77**, 014407 (2008).
- [19] R. Guo, L. E. Cross, S.-E. Park, B. Noheda, D. E. Cox, and G. Shirane, Origin of the high piezoelectric response in $PbZr_{1-x}Ti_xO_3$, *Phys. Rev. Lett.* **84**, 5423 (2000).
- [20] T. Ma, X. Liu, X. Pan, X. Li, Y. Jiang, M. Yan, H. Li, M. Fang, and X. Ren, Local rhombohedral symmetry in $Tb_{0.3}Dy_{0.7}Fe_2$

- near the morphotropic phase boundary, *Appl. Phys. Lett.* **105**, 192407 (2014).
- [21] Y. M. Jin, Domain microstructure evolution in magnetic shape memory alloys: Phase-field model and simulation, *Acta Mater.* **57**, 2488 (2009).
- [22] J. X. Zhang and L. Q. Chen, Phase-field microelasticity theory and micromagnetic simulations of domain structures in giant magnetostrictive materials, *Acta Mater.* **53**, 2845 (2005).
- [23] S. Rajput, X. Ke, X. Hu, M. Fang, D. Hu, F. Ye, Y. Hao, and X. Ren, Critical triple point as the origin of giant piezoelectricity in $\text{PbMg}_{1/3}\text{Nb}_{2/3}\text{O}_3\text{-PbTiO}_3$ system, *J. Appl. Phys.* **128**, 104105 (2020).
- [24] B. Noheda, D. E. Cox, G. Shirane, J. A. Gonzalo, L. E. Cross, and S.-E. Park, A monoclinic ferroelectric phase in the $\text{Pb}(\text{Zr}_{1-x}\text{Ti}_x)\text{O}_3$ solid solution, *Appl. Phys. Lett.* **74**, 2059 (1999).
- [25] U. Atzmony and M. P. Dariel, Nonmajor cubic symmetry axes of easy magnetization in rare-earth-iron Laves compounds, *Phys. Rev. B* **13**, 4006 (1976).
- [26] K. N. Martin, P. A. J. de Groot, B. D. Rainford, K. Wang, G. J. Bowden, J. P. Zimmermann, and H. Fangohr, Magnetic anisotropy in the cubic Laves REFe_2 intermetallic compounds, *J. Phys. Condens. Matter.* **18**, 459 (2006).
- [27] D. Vanderbilt and M. H. Cohen, Monoclinic and triclinic phases in higher-order Devonshire theory, *Phys. Rev. B* **63**, 094108 (2001).
- [28] X. Q. Ke, D. Wang, X. Ren, and Y. Wang, Formation of monoclinic nanodomains at the morphotropic phase boundary of ferroelectric systems, *Phys. Rev. B* **88**, 214105 (2013).
- [29] X. Q. Ke, D. Wang, and Y. Wang, Origin of ultrahigh piezoelectric activity of [001]-oriented ferroelectric single crystals at the morphotropic phase boundary, *Appl. Phys. Lett.* **108**, 012904 (2016).